Path-integral molecular dynamics simulation of diamond

Rafael Ramírez and Carlos P. Herrero

Instituto de Ciencia de Materiales, Consejo Superior de Investigaciones Científicas (CSIC), Campus de Cantoblanco, 28049 Madrid, Spain

Eduardo R. Hernández

Institut de Ciència de Materials de Barcelona (ICMAB), Consejo Superior de Investigaciones Científicas (CSIC), Campus de Bellaterra, 08193 Barcelona, Spain

Diamond is studied by path-integral molecular dynamics simulations of the atomic nuclei in combination with a tight-binding Hamiltonian to describe its electronic structure and total energy. This approach allows us to quantify the influence of quantum zero-point vibrations and finite temperatures on both the electronic and vibrational properties of diamond. The electron-phonon coupling mediated by the zero-point vibration reduces the direct electronic gap of diamond by 10%. The calculated decrease of the direct gap with temperature shows good agreement with the experimental data available up to 700 K. Anharmonic vibrational frequencies of the crystal have been obtained from a linear-response approach based on the path integral formalism. In particular, the temperature dependence of the zone-center optical phonon has been derived from the simulations. The anharmonicity of the interatomic potential produces a red shift of this phonon frequency. At temperatures above 500 K, this shift is overestimated in comparison to available experimental data. The predicted temperature shift of the elastic constant c_{44} displays reasonable agreement with the available experimental results.

PACS number(s): 63.20.Kr, 81.05.Uw, 63.20.Ry, 05.30.−d

I. INTRODUCTION

Tetrahedral semiconductors such as silicon, germanium, or diamond, have served as model materials to study the electronic and vibrational properties of crystals. In particular, the effects of the lattice vibrations on the electronic properties, through the mechanism of electron-phonon coupling, have been experimentally investigated by measuring the temperature dependence of their optical excitation spectra.[1] Furthermore, the observation of the dependence of such spectra with isotopic mass has provided detailed information on the electronic properties of these solids.[2] Besides the electron-phonon interaction, the anharmonicity of lattice vibrations has been observed by the dependence of the phonon frequencies and linewidths with temperature and isotopic composition.[2]

From a theoretical point of view, in spite of the impressive progress of *ab initio* methods for the investigation of the electronic structure of solids, the atomic nuclei are usually considered either as fixed in their crystallographic positions or by approximating their dynamics with classical mechanics.[3] Thus, the effects of the electron-phonon interactions on electronic properties and the effect of zero-point anharmonicity in the vibrational properties of the lattice are usually neglected in these calculations. As it has been pointed out in Ref. 1, these effects may be even larger that the error assumed in the electronic *ab initio* calculations.

The electron-phonon interaction in tetrahedral semiconductors has been studied theoretically by the perturbation theory.[4,5] Within this approach, the reduction of the direct electronic gap due to zero-point vibrations of the lattice phonons is predicted to be of 0.62 eV in diamond and of 0.06 eV in germanium. Both energy shifts represent roughly a 10% fraction of the corresponding energy gaps, i.e., they are so large that a quantitative description of the electronic

structure cannot be expected by a theory that neglects such effects. Anharmonic shifts of the phonon modes of diamond and silicon have been determined by combining the density-functional perturbation theory with a frozen-phonon approach,[6] and the results show good agreement with the experimental data available from first-order Raman spectra.[7,8] A review of the current status of lattice-dynamical calculations using the density-functional perturbation theory can be found in Ref. 9.

The path-integral (PI) formulation of statistical mechanics offers an alternative way to study finite temperature properties that are related to the quantum nature of the atomic nuclei.[10,11] Thus, the combination of the path-integral formulation with electronic structure methods is an interesting alternative to perturbational approaches for the study of electronic and vibrational properties of solids. An advantage of this approach is that both the electrons and the atomic nuclei are treated quantum mechanically in the framework of the Born-Oppenheimer (BO) approximation, so that anharmonic and temperature effects can be evaluated for both vibrational properties and the electronic structure. This unified scheme has been applied so far to the study of solids and molecules containing light atoms.[12–19]

In this paper we present a path integral molecular dynamics study of diamond at temperatures between 100 and 1200 K. The electronic structure has been treated by a nonorthogonal tight-binding (TB) Hamiltonian as a reasonable compromise to reduce the computational cost of deriving the BO surface for the nuclear dynamics. In particular, we are interested in the investigation of electronic properties that are determined by the electron-phonon coupling, as the dependence of the electronic gap with temperature and isotopic mass. Also vibrational properties that depend on the anharmonicity of the interatomic potential will be studied with the help of a linear response approach recently developed within

the path integral formalism.[20] PI simulations of diamond using effective interaction potentials have been carried out earlier to study structural and thermodynamic properties of this material.[21]

This paper is organized as follows. In Sec. II, we describe the computational method and the models employed in our simulations. Our results are presented and discussed in Sec. III, dealing with the direct electronic gap, the vibrational energy of the solid, and the temperature dependence of the frequency of the optical phonon at the center of the Brillouin zone (BZ) and the elastic constant c_{44} of diamond. In Sec. IV, we present the main conclusions of the paper.

II. COMPUTATIONAL METHOD

A. Simulation details

The formalism employed here for the quantum treatment of electrons and nuclei is based on the combination of the path-integral formulation, to derive properties of the atomic nuclei in thermal equilibrium, with an electronic Hamiltonian to derive the BO energy surface, $E_{BO}(\mathbf{R})$, as a function of the nuclear configuration $\mathbf{R}$. The path-integral and electronic structure parts of the resulting algorithm appear as independent blocks, since the only electronic result required for the path-integral simulation is the value of the function $E_{BO}(\mathbf{R})$, and possibly its derivatives with respect to ionic positions. Thus, the combination of path integrals with any chosen electronic Hamiltonian is straightforward. For the present investigation of diamond we have chosen an efficient tight-binding one-electron effective Hamiltonian, based on density functional (DF) calculations.[22] The use of a simplified electronic Hamiltonian is a reasonable compromise to explore the efficiency and capability of this unified formalism for the evaluation of electronic and vibrational properties of solids at finite temperatures. The implementation of density functional or Hartree-Fock based self-consistent methods is left for future development. The capability of tight-binding methods to simulate different properties of solids and molecules has been reviewed by Goringe et al.[23]

The computational advantage of using the path-integral formulation of statistical mechanics is formulated by the so-called "quantum-classical" isomorphism. Thus, this method exploits the fact that the partition function of a quantum system is formally equivalent to that of a classical one, obtained by replacing each quantum particle (here, atomic nucleus) by a ring polymer consisting of L "beads," connected by harmonic springs.[10,11,24,25] In many-body problems, the configuration space of the classical isomorph is usually sampled by Monte Carlo or molecular dynamics (MD) techniques. Here, we have employed the PI MD method, which has been found to require less computer time resources in our problem. Effective algorithms to perform PI MD simulations in the canonical NVT ensemble have been described in detail by Martyna et al.[26] and Tuckerman.[27] All calculations presented here were carried out in the canonical ensemble, using originally developed MD software, which enables efficient PI MD simulations on parallel supercomputers.
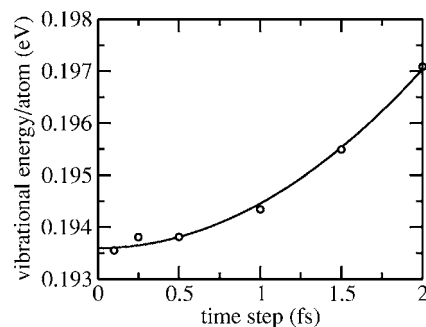

FIG. 1. Vibrational energy of diamond as a function of the time step, Δt, employed in the PI MD algorithm. The results are derived at 300 K with a Trotter number $L=20$. The continuous line is a quadratic fit to the simulation results.

Simulations were carried out on a $2 \times 2 \times 2$ supercell of the diamond face-centered-cubic cell with periodic boundary conditions, containing $N=64$ C atoms. The atomic mass of carbon was set to 12. The convergence of the internal energy has been checked for some selected atomic configurations, by considering sets of 1, 4, and 32 $\mathbf{k}$ points in the BZ of the simulation supercell. The main effect of the $\mathbf{k}$ point sampling is found to be a constant shift of the internal energy. This systematic error is largely reduced in the calculation of properties obtained as energy differences (e.g., energy shifts as a function of temperature). For this reason, we have chosen to use only the Γ point for the sampling of the BZ of the simulation supercell. A set of 4 $\mathbf{k}$ points increases the computer time by a factor of 10 with respect to the Γ point sampling, without significant changes of the results presented here.

The simulation-cell parameter employed in our calculations is taken from experimental data, and ranged from 7.1330 Å at 100 K to 7.1552 Å at 1200 K.[28] For a given temperature, a typical run consisted of 10^4 MD steps for system equilibration, followed by 5×10^5 steps for the calculation of ensemble average properties. To have a nearly constant precision in the path integral results at different temperatures, we have taken a number of beads, L (Trotter number), that scales with the inverse temperature such that $LT=6000$ K. For comparison with the results of our PI MD simulations, we have carried out some classical MD simulations with the same interatomic interaction (setting $L=1$). The quantum simulations were performed using a staging transformation for the bead coordinates. Chains of four Nosé-Hoover thermostats were coupled to each degree of freedom to generate the canonical ensemble.[29] To integrate the equations of motion we have used the reversible reference system propagator algorithm (RESPA), which allows one to define different time steps for the integration of the fast and slow degrees of freedom.[26] For the evolution of the fast dynamical variables, that include the thermostats and harmonic bead interactions, we used a time step $\delta t = \Delta t / 4$, where Δt is the time step associated to the calculation of DF-TB forces. The convergence of the total energy as a function of Δt is shown in Fig. 1. A value of $\Delta t = 0.5$ fs is found to provide adequate convergence. We have also explored the convergence of the simulation as a function of the thermostat mass, Q,
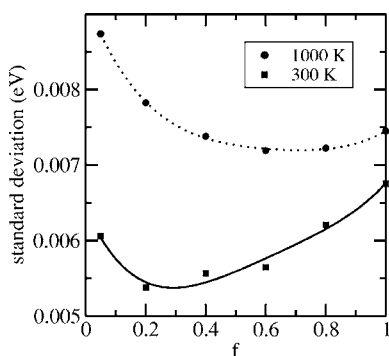
FIG. 2. Standard deviation of the total energy of the diamond supercell as a function of the scale factor f, used in Eq. (1) to define the thermostat mass, Q. The results correspond to simulation lengths of 10^5 MD steps at 300 K and 2×10^5 MD steps at 1000 K. The lines are guides to the eye.

$$Q = \frac{f\beta\hbar^2}{L}, \qquad (1)$$

where $\beta = (k_B T)^{-1}$ is the inverse temperature, and f is a scaling factor. The standard deviation of the total energy, as derived from a block analysis,[30] is displayed in Fig. 2 at two different temperatures. We observe that at 300 K the standard deviation can be reduced by about 20% by changing the f factor from a value of 1 to a value of 0.2. Taking into account that the standard deviation varies with the number of simulation steps, M_S, as $M_S^{-1/2}$, then, for a given threshold accuracy, a simulation run using $f = 0.2$ at 300 K requires 35% less simulation steps than a run using $f = 1$. In the simulations presented below, we have varied the parameter f linearly for temperatures between 300 and 1000 K. The f values changed from $f = 0.2$ (for $T \leqslant 300$ K) to $f = 1$ (for $T \geqslant 1000$ K).

B. Calculation of anharmonic vibrational frequencies

To calculate vibrational frequencies we will employ a method based on the linear response (LR) of the system to vanishingly small forces applied on the atomic nuclei. With this purpose, we consider a LR function, the static isothermal susceptibility χ^T, that is readily derived from PI MD simulations of the equilibrium solid, without having to explicitly impose any external forces during the simulation. This approach represents a significant improvement as compared to the standard harmonic (HA) approximation.[20] A sketch of the method is given in the following.

Let us call $\{\mathbf{R}_p\} = \{x_{ip}\}$ the set of $3NL$ Cartesian coordinates of the beads forming the ring polymers in the simulation cell ($i = 1, \ldots, 3N; p = 1, \ldots, L$). We consider the set $\{X_i\}$ of centroid coordinates, with X_i defined as the mean value of coordinate i over the corresponding polymer

$$X_i = \frac{1}{L}\sum_{p=1}^{L} x_{ip}. \qquad (2)$$

Then, the linear response of the quantum system to small external forces on the atomic nuclei is given by the suscep-

tibility tensor χ^T, which can be defined in terms of centroid coordinates as[20]

$$\chi_{ij}^T = \beta\sqrt{m_i m_j}\mu_{ij}, \qquad (3)$$

where $\beta = (k_B T)^{-1}$, m_i is the mass of the nucleus associated to coordinate i, $\mu_{ij} = \langle X_i X_j \rangle - \langle X_i \rangle \langle X_j \rangle$ is the covariance of the centroid coordinates X_i and X_j, and $\langle \cdots \rangle$ indicates an ensemble average along an MD run.

The tensor χ^T allows us to derive a LR approximation to the low-lying excitation energies of the vibrational system, that is applicable even to highly anharmonic situations. The LR approximation for the vibrational frequencies reads

$$\omega_{n,LR} = \frac{1}{\sqrt{\Delta_n}}, \qquad (4)$$

where Δ_n ($n = 1, \ldots, 3N$) are eigenvalues of χ^T, and the LR approximation to the low-lying excitation energy of vibrational mode n is given by $\hbar\omega_{n,LR}$. More details on the method and illustrations of its ability for predicting vibrational frequencies of solids and molecules can be found elsewhere.[20,31–33] In connection with the vibrational modes that actually appear in our calculations, we note that the application of periodic boundary conditions is physically equivalent to the consideration of lattice vibrations only at the center ($\mathbf{k} = \mathbf{0}$) of the BZ of the employed *simulation cell*. Modes with $\mathbf{k} \neq \mathbf{0}$ violate the periodic boundary conditions, because all atomic images of an atom have distinct displacements, whose amplitude is modulated by both the propagation vector $\mathbf{k}$ of the vibrational mode and the translational vector of the image. However, periodic boundary conditions implies that all atomic images must display a displacement identical to that one of the atom located in the simulation cell, a condition that is only met if the propagation vector is $\mathbf{k} = \mathbf{0}$.[33]

C. Calculation of one-electron energies

For the sake of clarity, we use the Schrödinger formulation to derive the expectation value of electronic observables. However, the final result is obtained in a form appropriate to the path integral formulation. Within the adiabatic Born-Oppenheimer approximation,[34] the total wave function is written as

$$\Psi_i(\mathbf{r}, \mathbf{R}) = \chi_i(\mathbf{R})\varphi_0(\mathbf{r}, \mathbf{R}), \qquad (5)$$

where $(\mathbf{r}, \mathbf{R})$ are the electronic and nuclear coordinates, χ_i labels the nuclear wave function, and φ_0 represents the electronic ground state configuration, which depends parametrically on $\mathbf{R}$. Let us call ϵ_i the energy of the state Ψ_i. Then, the canonical partition function, Z, is defined as

$$Z = \sum_i e^{-\beta\epsilon_i}. \qquad (6)$$

We consider an electronic observable represented by the operator $\mathcal{E}(\mathbf{r}, \mathbf{R})$, that is a function of the electronic coordinates and depends parametrically on $\mathbf{R}$. Its canonical average, $\langle E \rangle$, is defined as

$$\langle E \rangle = Z^{-1} \sum_i e^{-\beta \epsilon_i} \int d\mathbf{R} \int d\mathbf{r} \, \Psi_i^*(\mathbf{r}, \mathbf{R}) \mathcal{E}(\mathbf{r}, \mathbf{R}) \Psi_i(\mathbf{r}, \mathbf{R}).$$

$$(7)$$

Now, we write this equation in an alternative way, better adapted to the path integral formulation. First, the function $E(\mathbf{R})$ is defined as the expectation value of the operator $\mathcal{E}(\mathbf{r}, \mathbf{R})$ over the electronic wave function

$$E(\mathbf{R}) = \int d\mathbf{r} \, \varphi_0^*(\mathbf{r}, \mathbf{R}) \mathcal{E}(\mathbf{r}, \mathbf{R}) \varphi_0(\mathbf{r}, \mathbf{R}). \qquad (8)$$

The second definition is the funtion $\rho(\mathbf{R}, \mathbf{R})$, representing the diagonal elements of the normalized canonical density matrix for the nuclear coordinates

$$\rho(\mathbf{R}, \mathbf{R}) = Z^{-1} \sum_i e^{-\beta \epsilon_i} |\chi_i(\mathbf{R})|^2. \qquad (9)$$

Considering the factorization of $\Psi_i(\mathbf{r}, \mathbf{R})$ in Eq. (5), and using the last two definitions, we can rewrite the average $\langle E \rangle$ in Eq. (7) as

$$\langle E \rangle = \int d\mathbf{R} \, \rho(\mathbf{R}, \mathbf{R}) E(\mathbf{R}). \qquad (10)$$

The last equation shows that electronic observables, $\langle E \rangle$, are obtained as ensemble averages over the nuclear configurations, $\mathbf{R}$, accessible in thermal equilibrium. This equation can be readily used in combination with the path integral sampling of the density matrix $\rho(\mathbf{R}, \mathbf{R})$. We will apply it to calculate the canonical average, $\langle E_n \rangle$, of the nth energy eigenvalue of the electronic Hamiltonian. For convenience, let us define the following probability density for the one-electron state E_n,

$$\rho_n(E) = \int d\mathbf{R} \, \rho(\mathbf{R}, \mathbf{R}) \delta[E_n(\mathbf{R}) - E], \qquad (11)$$

where δ is the Dirac delta function. $\rho_n(E)$ can be easily accumulated during a PI MD simulation. The expectation value, $\langle E_n \rangle$, as given by Eq. (10), can now be written as the first moment of the distribution ρ_n,

$$\langle E_n \rangle = \int dE \, \rho_n(E) E. \qquad (12)$$

The direct electronic gap of diamond is derived as

$$E_g = \langle E_c \rangle - \langle E_v \rangle, \qquad (13)$$

where E_c and E_v are the one-electron states associated with the bottom of the conduction band and the top of the valence band at the reciprocal point $\mathbf{k} = 0$.

III. RESULTS AND DISCUSSION

In this section we present the main results derived from our PI MD simulations of diamond as a function of temperature. Whenever possible we will compare the simulation results to available experimental data. Results concerning the
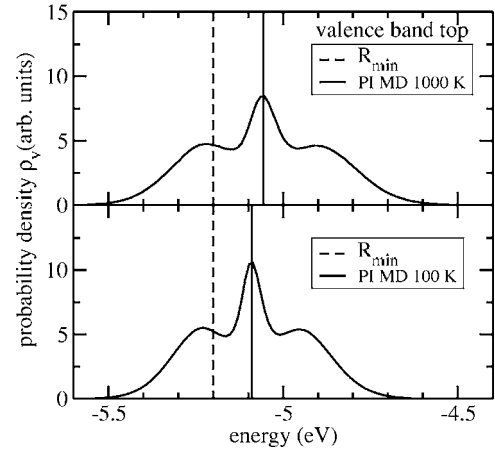

FIG. 3. Probability density functions for the valence band top of diamond obtained by PI MD simulations at 100 and 1000 K. The expectation value of the electronic level, $\langle E_v \rangle$, is shown as a vertical continuous line. The broken line shows the valence band top, E_v, for the nuclear configuration $\mathbf{R}_{\min}$, with the atoms fixed at their crystallographic positions and the cell parameter fixed at the equilibrium value at 100 K.

electronic and vibrational properties are presented in the next subsections.

A. Electronic properties

1. One-electron states

The top of the valence band, E_v, for a diamond crystal with the atoms fixed in their crystallographic positions, $\mathbf{R}_{\min}$, is threefold degenerate. Each of these three one-electron levels leads to identical probability densities, ρ_v, as defined in Eq. (11). The function $\rho_v(E)$, derived from our PI MD simulations, is represented in Fig. 3 at two temperatures, 100 and 1000 K. The probability density shows three distinct maxima reflecting that the underlying electronic state is threefold degenerate. In each case, the continuous vertical line displays the expectation value of the valence band top, $\langle E_v \rangle$, defined as the first moment of the distribution ρ_v [see Eq. (12)]. The temperature effect in $\langle E_v \rangle$ is a shift of 0.03 eV toward higher energies, when the temperature increases from 100 to 1000 K. This shift is a consequence of the different magnitude of the electron-phonon interaction at both temperatures (longer atomic displacements at higher T). The dotted line in the figure represents the energy of the top of the valence band, E_v, for a crystal with atoms fixed at their equilibrium positions and cell parameter set to the equilibrium value at $T = 100$ K ($a = 3.5665$ Å). The PI MD simulation predicts that at 100 K the top of the valence band is shifted by 0.11 eV with respect to the result obtained for the $\mathbf{R}_{\min}$ configuration.

In Fig. 4 we present the results corresponding to the one-electron state E_c, i.e., the conduction band bottom at the reciprocal point $\mathbf{k} = 0$. The energy shifts found for E_c as a consequence of the electron-phonon interaction are larger and of opposite sign as those encountered for the valence band. At 100 K we observe a downwards shift of $\langle E_c \rangle$ by
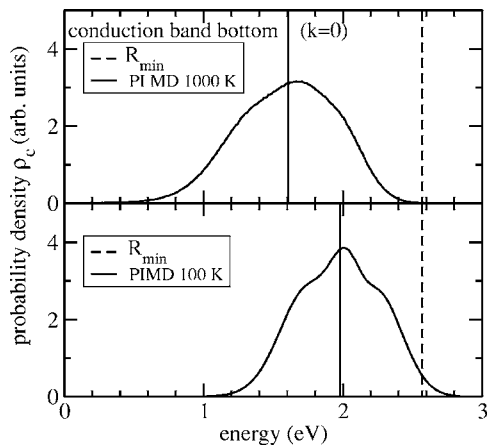
FIG. 4. Probability density function for the conduction band bottom at the reciprocal point $\mathbf{k}=\mathbf{0}$, obtained by PI MD simulations at 100 and 1000 K. The expectation value for this electronic level, $\langle E_c \rangle$, is shown by a continuous vertical line. The broken line shows the position of E_c for the static nuclear configuration $\mathbf{R}_{min}$.

about -0.59 eV with respect to the $\mathbf{R}_{min}$ configuration. The temperature shift in $\langle E_c \rangle$ amounts to -0.37 eV between 100 and 1000 K.

2. Direct electronic gap

The first direct gap, $E_g = \langle E_c \rangle - \langle E_v \rangle$, of diamond has been portrayed in Fig. 5 as a function of temperature. The open circles have been derived from PI MD simulations where the thermal expansion of the crystal lattice has been taken into account by varying the value of the cell parameter a. Open squares are PI MD results derived at different temperatures with a cell parameter fixed at the equilibrium value at 100 K. We note that the effect of the thermal expansion on the electronic gap is a slight reduction of the gap. The temperature dependence of the electronic gap predicted by our PI MD
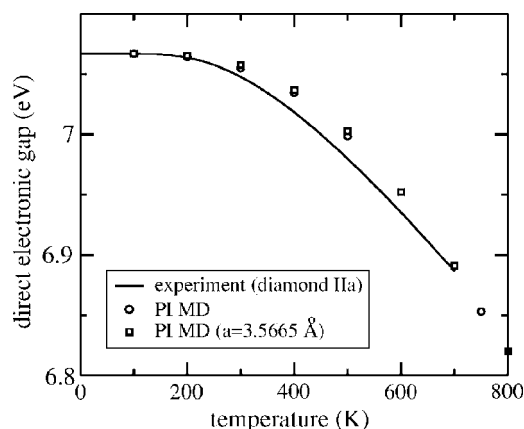

FIG. 5. Temperature dependence of the direct electronic gap of diamond obtained by our PI MD simulations. Open circles were derived from simulations that take into account the thermal expansion of the lattice. Open squares correspond to simulations where the cell parameter was fixed to the equilibrium value at 100 K. The continuous line is the fit to the experimental data given in Ref. 35 for diamond IIa.
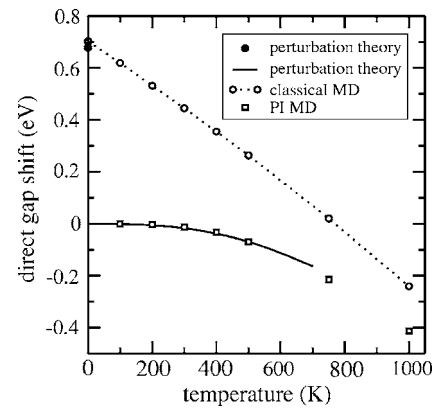

FIG. 6. Relative shifts of the direct electronic gap of diamond. Open circles are results from classical MD simulations, while open squares correspond to quantum PI MD simulations. The solid circle at $T=0$ and the continuous line are results presented in Ref. 5 based on perturbation theory. For both PI MD simulations and perturbation theory, shifts are given with respect to the corresponding quantum limit at $T=0$. The dotted line is a guide to the eye.

simulations is in reasonable agreement with the experimental results reported in Ref. 35 for diamond IIa up to 700 K, based on measurements of the complex dielectric function by spectroscopic ellipsometry. The slope of the simulation results at temperatures above 500 K is larger than that of the experimental data. A possible reason for this behavior is an overestimation of anharmonic effects by the DF-TB potential model. Although we expected a reasonable agreement between experimental and theoretical results at low T, the coincidence shown in Fig. 5 for the absolute value of the first direct gap is fortuitous. In fact, the displayed experimental values, derived from first-derivative line shape analysis of the complex dielectric function, are shifted by about 0.07 eV toward higher energies, in case that they are obtained by second-derivative line-shape analysis.[35]

To quantify the influence of nuclear quantum effects on the value of the direct electronic gap of diamond we have performed a series of classical MD simulations as a function of temperature. The shifts of the energy gap obtained in the classical simulations are compared to the PI MD results in Fig. 6. The most prominent quantum effect appears in the low temperature limit as a consequence of the zero-point vibration. The renormalization of E_g amounts to 0.7 eV at $T=0$. This value agrees well with the perturbational treatment of the electron-phonon coupling in Ref. 5, whose result is represented by a closed circle in Fig. 6. We stress that the zero-point renormalization of E_g amounts to about 10% of its value. The PI MD results show satisfactory agreement with the perturbation theory data available up to 700 K.[5] The main discrepancy found between both sets of results is that the slope at temperatures above 500 K is larger for PI MD than for the perturbation theory. The overestimation of anharmonic effects by the DF-TB model is a probable explanation for this behavior. Differences between the quantum and classical results for E_g are significant in the whole studied temperature range. In particular, at room temperature the classical result deviates from the PI MD data by about 0.45 eV.
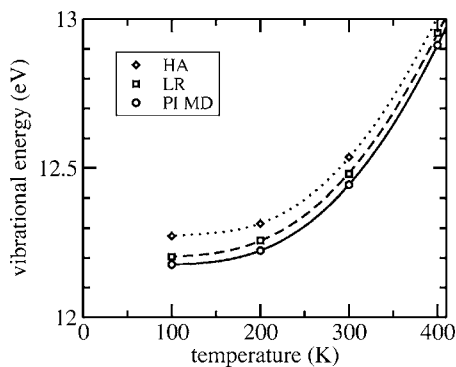
FIG. 7. The vibrational energy of the simulation cell of diamond as a function of temperature is shown by open circles. The zero of energy corresponds to the crystal with fixed atoms and cell parameter $a=3.5665$ Å. The harmonic vibrational energy derived from the set of harmonic and linear response frequencies is displayed as open diamonds and squares, respectively. The lines are guides to the eye.

We have calculated the shift of the direct electronic gap of diamond as a function of the isotopic mass at 300 K. The calculated energy gap for ^{12}C amounts to 7.054 eV. For ^{13}C, this gap increases to 7.081 eV at the same temperature. The isotopic effect of 27 meV at 300 K is in reasonable agreement to the value reported in Ref. 5 of 22 meV, based on perturbation theory in the zero temperature limit.

B. Vibrational properties

1. Vibrational energy

The vibrational energy of the simulation cell of diamond, as derived by the PI MD simulations, is presented as a function of temperature in Fig. 7 (solid circles). The zero of the energy scale corresponds to a diamond crystal with fixed atoms and with the cell parameter fixed at the equilibrium value at 100 K. The thermal occupation of excited vibrational states is evident in Fig. 7 by the increase of the vibrational energy with temperature. To quantify the anharmonic effect on the vibrational energy of the crystal, we have plotted in Fig. 7 the harmonic vibrational energy (solid diamonds). The set of harmonic frequencies has been derived by diagonalizing the dynamic matrix in a simulation cell with the experimental equilibrium lattice parameter at each temperature. At the lowest studied temperature the harmonic result deviates from the PI MD value by about 0.1 eV, which amounts to about 0.8% of the total vibrational energy. This error of the harmonic approximation is a consequence of the anharmonicity of the phonon vibrations.

The set of anharmonic vibrational frequencies, $\omega_{n,LR}$, derived by our linear response approach, are expected to represent an improved description of the vibrational problem. Thus, we have recalculated the harmonic vibrational energy by considering $\omega_{n,LR}$ as a set of renormalized phonon frequencies. The result is shown as open squares in Fig. 7. Most of the error of the harmonic approximation is corrected by the LR frequencies. At low temperatures the absolute error of the improved estimation of the vibrational energy amounts to
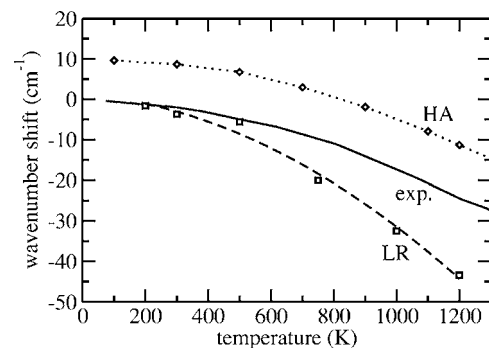

FIG. 8. Temperature shift of the optical phonon at Γ ($\mathbf{k}=\mathbf{0}$) of diamond. The results of the LR and harmonic approximations are compared with a fit to the experimental data of Ref. 7. The extrapolated LR value at $T=0$ has been employed as zero of the vertical axis for both the LR and HA results. The zero of the experimental data corresponds to the extrapolated experimental wavenumber at $T=0$.

0.03 eV, i.e., about 0.2% of the PI MD result. Our conclusion from this comparison is that the set of LR frequencies provides a consistent description of anharmonic effects in the employed DF-TB model, in line with previous results of vibrational properties on molecular and solid state systems.[20,32,33] In the following, we focus on the study of two particular LR phonons that can be compared to available experimental data.

2. Optical phonon at k=0

The highest energy phonon of the diamond crystal is the optical phonon at the center of the BZ ($\mathbf{k}=\mathbf{0}$). At 200 K, the LR wave number of this phonon amounts to 1396 ± 5 cm^{-1}. The harmonic result, obtained for the equilibrium cell parameter at this temperature, is 1407 cm^{-1}. The difference between the LR and harmonic result is a consequence of the anharmonicity of the interatomic potential that induces a slight softening in the phonon frequency. The optical phonon wavenumber of diamond in the zero temperature limit is found in the first-order Raman spectrum at 1335 cm^{-1}.[7] The DF-TB potential overestimates the experimental wave number by about 61 cm^{-1}. This error is lower than that found in other tight-binding parametrizations.[36,37]

The relative shift of the optical phonon in diamond is presented as a function of temperature in Fig. 8. The comparison between the harmonic and LR results shows that anharmonic effects lead to a softening of the phonon mode in the studied temperature range up to 1200 K. The LR results deviate from the experimental data at temperatures above 500 K. This deviation shows that the anharmonicity of the optical phonon is overestimated by the DF-TB Hamiltonian at those temperatures. We have previously commented on the enhanced anharmonicity of the DF-TB model in relation to the decrease of the direct electronic gap at temperatures above 500 K.

3. Elastic constant c_{44}

The lowest energy phonon, ω_1, determined by either the LR or HA approximations is 12-fold degenerated in the em-
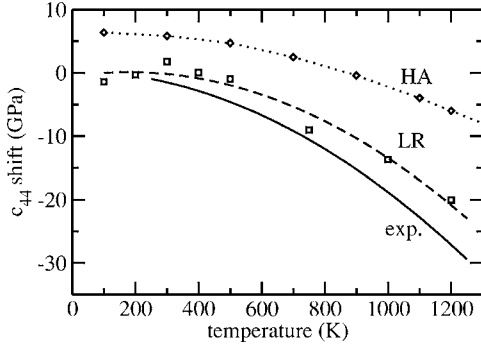
FIG. 9. Temperature shift of the elastic constant c_{44} of diamond. The results of the LR and harmonic approximations are compared to a fit to the experimental data of Ref. 38. The extrapolated LR value at $T=0$ has been employed as zero of the vertical axis for both the LR and HA results. The zero of the experimental data corresponds to the extrapolated experimental constant at $T=0$.

ployed simulation cell. The wave vector, $\mathbf{k}_1$, of this phonon state has been identified as the midpoint between Γ and X points along the $\Delta[100]$ direction in reciprocal space, with coordinates $(\pi/a, 0, 0)$. This means that the phonon ω_1 corresponds to the TA branch. The identification of the wave vector of ω_1 has been possible by solving the dynamical matrix at some selected $\mathbf{k}$ points of the BZ of the primitive unit cell of diamond. The phonon velocity, v_{TA}, along the TA branch, $\omega_{TA}(k_{TA})$, is defined as the slope of the dispersion branch at the origin

$$v_{TA} = \lim_{k_{TA} \to 0} \frac{\omega_{TA}}{k_{TA}} \approx c \frac{\omega_1}{k_1}. \tag{14}$$

In this equation, $k_1 = \pi/a$ is the modulus of the wave vector $\mathbf{k}_1$ associated to the phonon ω_1. The constant $c = 1.037$ corrects, for the case of the HA approximation, the finite difference error encountered by using the finite vector $\mathbf{k}_1$ to calculate the slope at the origin. The elastic constant c_{44} can be derived from v_{TA} by the relation

$$c_{44} = \rho v_{TA}^2, \tag{15}$$

where ρ is the density of the diamond crystal.

Using the harmonic value of $\omega_{1,HA}$ at 200 K we obtain with Eqs. (14) and (15) a value for c_{44} of 551 GPa. The estimation of the elastic constant using the LR wave number, $\omega_{1,LR}$, in Eq. (14) is of 545 GPa. The experimental result derived from Brillouin scattering amounts to 576 GPa.[38] The shift of the elastic constant c_{44} with temperature is plotted in Fig. 9. The comparison of the LR and harmonic results shows that anharmonic effects cause a reduction of the value of the elastic constant c_{44} in the whole studied temperature range. The comparison to the experimental data shows that the DF-TB model gives a reasonable prediction of the temperature shift of the c_{44} elastic constant, even though there appears a systematic underestimation of this shift.

IV. CONCLUSIONS

The simulations presented here for diamond are based on the treatment of electrons and nuclei as quantum particles in the framework of the Born-Oppenheimer approximation. The use of the path integral formulation for the atomic nuclei allows us to obtain the vibrational and electronic properties of the solid at finite temperatures. We have chosen a simplified electronic Hamiltonian to develop the algorithms required for the simulation of solid state systems, but this limitation should be eliminated in the future by the implementation of improved electronic structure methods.

The temperature and isotopic dependence of the first direct gap of diamond predicted by our PI MD simulation shows good agreement with the available experimental results, based on spectroscopic ellipsometry,[35] and theoretical results, based on perturbation theory.[5] Thus, the employed simulation model has demonstrated its capability to realistically describe electronic properties that are determined by electron-phonon interactions. The effect of the zero point vibrations of the lattice phonons of diamond in its first direct gap is a reduction of the gap by about 0.7 eV. This effect is so large that any theoretical approach aiming at a quantitative determination of the electronic gap of diamond can not be based only on an improved solution of the many-body electronic problem, but it should also include the treatment of the electron-phonon coupling.

Anharmonic effects in the lattice vibrations have been derived by a linear response approach based on the path integral formulation. This approach allows us to derive anharmonic vibrational frequencies from the study of spatial correlations in the displacements of the vibrating nuclei in the simulation cell. Anharmonic effects are responsible for a reduction of the vibrational energy of the solid of about 1%, with respect to the result predicted by a harmonic approximation. The temperature shift of the optical phonon at $\mathbf{k}=0$ is larger that the experimental result determined by Raman spectroscopy.[7] We consider that this limitation is a consequence of the parametrization of the employed DF-TB one-electron Hamiltonian,[22] that overestimates the anharmonicity of the highest frequency phonon of the lattice. Better agreement is found in the comparison of the elastic constant c_{44} derived from the simulations with the experimental values obtained by Brillouin scattering.[38]

We plan to extend our simulations to more complex systems like hydrogen impurities in diamond,[39] where the presence of light impurities should strengthen further the influence of quantum nuclear effects in the electronic and vibrational properties of the lattice.

[1] M. Cardona, Solid State Commun. **133**, 3 (2005).

[2] M. Cardona and M. L. W. Thewalt, Rev. Mod. Phys. **77**, 1173 (2005).

[3] R. Car and M. Parrinello, Phys. Rev. Lett. **55**, 2471 (1985).

[4] P. B. Allen and M. Cardona, Phys. Rev. B **23**, 1495 (1981).

[5] S. Zollner, M. Cardona, and S. Gopalan, Phys. Rev. B **45**, 3376 (1992).

[6] G. Lang, K. Karch, M. Schmitt, P. Pavone, A. P. Mayer, R. K. Wehner, and D. Strauch, Phys. Rev. B **59**, 6182 (1999).

[7] H. Herchen and M. A. Cappelli, Phys. Rev. B **43**, 11740 (1991).

[8] D. Schiferl, M. Nicol, J. M. Zaug, S. K. Sharma, T. F. Cooney, S. Y. Wang, T. R. Anthony, and J. F. Fleischer, J. Appl. Phys. **82**, 3256 (1997).

[9] S. Baroni, S. de Gironcoli, and A. D. Corso, Rev. Mod. Phys. **73**, 515 (2001).

[10] R. P. Feynman, *Statistical Mechanics* (Addison-Wesley, New York, 1972).

[11] D. M. Ceperley, Rev. Mod. Phys. **67**, 279 (1995).

[12] M. E. Tuckerman, D. Marx, M. L. Klein, and M. Parrinello, Science **275**, 817 (1997).

[13] M. Shiga, M. Tachikawa, and S. Miura, J. Chem. Phys. **115**, 9149 (2001).

[14] M. Tachikawa and M. Shiga, Chem. Phys. Lett. **407**, 135 (2005).

[15] B. Chen, I. Ivanov, M. L. Klein, and M. Parrinello, Phys. Rev. Lett. **91**, 215503 (2003).

[16] F. Della Sala, R. Rousseau, A. Görling, and D. Marx, Phys. Rev. Lett. **92**, 183401 (2004).

[17] Y. Ohta, K. Ohta, and K. Kinugawa, J. Chem. Phys. **121**, 10991 (2004).

[18] R. Ramírez, E. Hernández, J. Schulte, and M. C. Böhm, Chem. Phys. Lett. **291**, 44 (1998).

[19] D. Marx and M. Parrinello, Science **271**, 179 (1996).

[20] R. Ramírez and T. López-Ciudad, J. Chem. Phys. **115**, 103 (2001).

[21] C. P. Herrero and R. Ramírez, Phys. Rev. B **63**, 024103 (2001).

[22] D. Porezag, T. Frauenheim, T. Köhler, G. Seifert, and R. Kaschner, Phys. Rev. B **51**, 12947 (1995).

[23] C. M. Goringe, D. R. Bowler, and E. Hernández, Rep. Prog. Phys. **60**, 1447 (1997).

[24] M. J. Gillan, Philos. Mag. A **58**, 257 (1988).

[25] H. Kleinert, *Path Integrals in Quantum Mechanics, Statistics and Polymer Physics* (World Scientific, Singapore, 1990).

[26] G. J. Martyna, M. E. Tuckerman, D. J. Tobias, and M. L. Klein, Mater. Chem. Phys. **87**, 1117 (1996).

[27] M. E. Tuckerman, in *Quantum Simulations of Complex Many-Body Systems: From Theory to Algorithms*, edited by J. Grotendorst, D. Marx, and A. Muramatsu (NIC, FZ Jülich, 2002), p. 269.

[28] B. J. Skinner, Am. Mineral. **42**, 39 (1957).

[29] M. E. Tuckerman and A. Hughes, in *Classical & Quantum Dynamics in Condensed Phase Simulations*, edited by B. J. Berne, G. Ciccotti, and D. F. Coker (World Scientific, Singapore, 1998), p. 311.

[30] J. Cao and B. J. Berne, J. Chem. Phys. **91**, 6359 (1989).

[31] R. Ramírez and T. López-Ciudad, in *Quantum Simulations of Complex Many-Body Systems: From Theory to Algorithms*, edited by J. Grotendorst, D. Marx, and A. Muramatsu (NIC, FZ Jülich, 2002), pp. 325–375; for downloads and audiovisual Lecture Notes, see www.theochem.rub.de/go/cprev.html.

[32] T. López-Ciudad, R. Ramírez, J. Schulte, and M. C. Böhm, J. Chem. Phys. **119**, 4328 (2003).

[33] R. Ramírez and C. P. Herrero, Phys. Rev. B **72**, 024303 (2005).

[34] G. Fischer, in *Vibronic Processes in Inorganic Chemistry*, edited by C. D. Flint (Kluwer, Dordrecht, 1989), p. 7.

[35] S. Logothetidis, J. Petalas, H. M. Polatoglou, and D. Fuchs, Phys. Rev. B **46**, 4483 (1992).

[36] C. Z. Wang, C. T. Chan, and K. M. Ho, Phys. Rev. B **42**, 11276 (1990).

[37] G. Kopidakis, C. Z. Wang, C. M. Soukoulis, and K. M. Ho, J. Phys.: Condens. Matter **9**, 7071 (1997).

[38] E. S. Zouboulis, M. Grimsditch, A. K. Ramdas, and S. Rodriguez, Phys. Rev. B **57**, 2889 (1998).

[39] C. P. Herrero, R. Ramírez, and E. R. Hernández (unpublished).